



THE UNIVERSITY *of* EDINBURGH

Edinburgh Research Explorer

Dual-Enhanced Photocatalytic Activity of Fe-Deposited Titanate Nanotubes Used for Simultaneous Removal of As(III) and As(V)

Citation for published version:

Borthwick, A, Liu, W, Wang, Y, Zhao, X & Ni, J 2015, 'Dual-Enhanced Photocatalytic Activity of Fe-Deposited Titanate Nanotubes Used for Simultaneous Removal of As(III) and As(V)', *ACS Applied Materials & Interfaces*, pp. 19726-19735. <https://doi.org/10.1021/acsami.5b05263>

Digital Object Identifier (DOI):

[10.1021/acsami.5b05263](https://doi.org/10.1021/acsami.5b05263)

Link:

[Link to publication record in Edinburgh Research Explorer](#)

Document Version:

Peer reviewed version

Published In:

ACS Applied Materials & Interfaces

General rights

Copyright for the publications made accessible via the Edinburgh Research Explorer is retained by the author(s) and / or other copyright owners and it is a condition of accessing these publications that users recognise and abide by the legal requirements associated with these rights.

Take down policy

The University of Edinburgh has made every reasonable effort to ensure that Edinburgh Research Explorer content complies with UK legislation. If you believe that the public display of this file breaches copyright please contact openaccess@ed.ac.uk providing details, and we will remove access to the work immediately and investigate your claim.



This document is confidential and is proprietary to the American Chemical Society and its authors. Do not copy or disclose without written permission. If you have received this item in error, notify the sender and delete all copies.

Dual-Enhanced Photocatalytic Activity of Fe-Deposited Titanate Nanotubes Used for Simultaneous Removal of As(III) and As(V)

Journal:	<i>ACS Applied Materials & Interfaces</i>
Manuscript ID:	am-2015-052632.R3
Manuscript Type:	Article
Date Submitted by the Author:	15-Aug-2015
Complete List of Authors:	Liu, Wen; The Key Laboratory of Water and Sediment Sciences, Ministry of Education, Department of Environmental Engineering ZHAO, XIAO; Auburn University, Civil Engineering Borthwick, Alistair; Institute of Energy Systems, School of Engineering, Wang, Yanqi; The Key Laboratory of Water and Sediment Sciences, Ministry of Education, Department of Environmental Engineering Ni, Jinren; Peking University, Dept. of Environmental Engineering

SCHOLARONE™
Manuscripts

1
2
3
4
5 **Dual-Enhanced Photocatalytic Activity of Fe-Deposited Titanate**
6
7
8 **Nanotubes Used for Simultaneous Removal of As(III) and As(V)**
9

10
11 Wen Liu,^{†,‡} Xiao Zhao,[‡] Alistair G.L. Borthwick,[§] Yanqi Wang,[†] Jinren Ni^{*,†}
12

13
14 [†] *The Key Laboratory of Water and Sediment Sciences, Ministry of Education, Department of*
15 *Environmental Engineering, Peking University, Beijing 100871, China*
16

17 [‡] *Environmental Engineering Program, Department of Civil Engineering, Auburn University,*
18 *Auburn, AL 36849, United States*
19

20 [§] *Institute of Energy Systems, School of Engineering, The University of Edinburgh, The King's*
21 *Buildings, Edinburgh EH9 3JL, UK*
22
23
24
25
26
27
28
29
30
31
32
33
34
35
36
37
38
39
40
41
42
43
44
45
46
47
48
49
50
51
52
53
54
55
56
57
58
59
60

ABSTRACT

Fe-deposited titanate nanotubes (Fe-TNTs) with high photocatalytic activity and adsorptive performance were synthesized through a one-step hydrothermal method. Initial As(III) oxidation followed by As(V) adsorption by Fe-TNTs could simultaneously remove these two toxic pollutants from aqueous solutions. The apparent rate constant value for photo-oxidation of As(III) under UV irradiation by Fe-TNTs was almost 250 times that by unmodified TNTs. Under visible light, the Fe-TNTs also exhibited enhanced photocatalytic activity after Fe was deposited. Fe³⁺ located in the interlayers of TNTs acted as temporary electron- or hole-trapping sites, and attached α -Fe₂O₃ played the role of a charge carrier for electrons transferred from TNTs. These two effects inhibited electron-hole pair recombination thus promoting photocatalysis. Moreover, the As(V) adsorptive performance of Fe-TNTs also improved, owing to the presence of additional adsorption sites, α -Fe₂O₃, as well as increased p*H*_{PZC}. Furthermore, Fe-TNTs exhibited good photocatalytic and adsorptive performance even after 5 reuse cycles. The present tests, concerning an initial As(III) photocatalysis and subsequent As(V) adsorption process, highlight the feasibility and importance of Fe used to modify TNTs. This study proposes a feasible method to simultaneously remove As(III) and As(V) from contaminated water using a novel Ti-based nanomaterial.

KEYWORDS: titanate nanotubes; Fe deposited; photocatalytic activity; dual-enhanced; visible light; As

1. INTRODUCTION

TiO₂-devised nanomaterials are increasingly applied as photocatalysts and adsorbents in environmental remediation.¹⁻⁴ One-dimensional (1D) nanostructure based materials are considered promising materials for photocatalytic application.^{5,6} Specifically, 1D hydrothermally-prepared titanate nanotubes (TNTs) are widely used as heavy-metal adsorbents due to their excellent ion-exchange characteristics, large surface area, and abundant functional groups (-OH).⁷⁻⁹ However, not like their precursor, TiO₂, raw TNTs show weak photocatalytic activity due to the rapid recombination of excited electrons and holes after irradiation.^{3, 10-12} Consequently, there has been a recent upsurge in the number of research studies on the modification of TNTs to enhance their photocatalytic activity. Certain studies focus on the phase transition from titanate to TiO₂ by means of acid or heat treatment,^{10, 13, 14} which can only enhance the photocatalytic activity under UV light and no studies about response on visible light by calcined or hydrogen TNTs were reported. Others consider deposition of transition or precious metals (e.g. Cu, Pd, W, Au, CdS and etc.) onto TNTs so as to inhibit the recombination of electron-hole pairs by creating a new donor level, which can help to transfer the excited electrons.¹⁵⁻¹⁸ In addition, light adsorption edge to visible range was also observed after metal deposition.^{16, 18} Therefore, metal deposition is more energy-efficient and easier to undertake for modification of TNTs than phase transition, especially for low-cost, common metals (like Cu and Fe) deposition.

1
2
3
4 Arsenic (As) is a highly toxic and carcinogenic pollutant whose presence in the
5
6 water environment can present a major threat to the eco-system and human beings
7
8 through accumulation in the food chain.^{19, 20} The International Agency for Research
9
10 on Cancer (IARC) recognizes arsenic and arsenic compounds as group 1 carcinogens,
11
12 and the EU lists arsenic trioxide, arsenic pentoxide and arsenate salts as category 1
13
14 carcinogens.²¹ Two main forms of As are found in water, As(III) and As(V). Of these
15
16 As(III) exhibits much higher toxicity than As(V) because of its high affinity to thiols,
17
18 the active sites of many important enzymes in living bodies.²² So a common technique
19
20 for removal of As from aqueous solutions involves oxidation of As(III) to As(V) to
21
22 reduce toxicity first, followed by further treatment to achieve complete removal.^{23, 24}
23
24 Although iron oxides, such as Fe₂O₃ and Fe₃O₄, have been found to be some of the
25
26 best materials for As removal,^{25, 26} operational bottlenecks occur due to the oxidation
27
28 efficiency of As(III) and adsorption capacity of As(III) or As(V). However, the
29
30 excellent adsorption and photocatalytic characteristics of modified TNTs imply they
31
32 may play an important role in As removal.^{4, 27-29} Given the large capacity of Fe oxides
33
34 for As adsorption, Fe-deposited TNTs with enhanced photocatalytic and adsorptive
35
36 property compare with TNTs would appear to be a good choice for removing As from
37
38 aqueous solutions.
39
40
41
42
43
44
45
46
47

48
49 In the present study, a novel Fe-deposited titanate nanotubes (Fe-TNTs) were
50
51 synthesized through a one-step hydrothermal method. Both photocatalytic activity and
52
53 adsorption performance of the Fe-TNTs were greatly enhanced compared to
54
55 conventional TNTs. The new material was detailly characterized and the role of Fe in
56
57
58
59
60

1
2
3
4 enhancement of the photocatalytic activity and adsorptive performance were
5
6 intercepted. The main objective is to achieve simultaneous removal of As(III) and
7
8 As(V) through initial photocatalysis (especially under visible light) and subsequent
9
10 adsorption using Fe-TNTs. A full discussion is included on the key role played by Fe
11
12 as a deposited element in modifying the TNTs used to remove As(III) and As(V).
13
14
15
16

17 **2. EXPERIMENTAL SECTION**

19
20 **2.1. Chemicals.** All chemicals were of analytical grade and did not require
21
22 further purification. TiO₂ nanoparticles (P25, 80% anatase and 20% rutile) were
23
24 purchased from Degussa Corporation of Germany. FeCl₃·6H₂O, NaOH and absolute
25
26 ethanol (also used to synthesize Fe-TNTs) were obtained from Tianjin Fuchen
27
28 Chemical Company, China. High-purity deionized (DI) water (Millipore Co., 18.2
29
30 MΩ·cm) was used to prepare all solutions. NaAsO₂ and Na₂HAsO₄·7H₂O
31
32 (Sigma-Aldrich Co., USA) were respectively used to prepare As(III) and As(V) stock
33
34 solutions (each of 100 mg L⁻¹).
35
36
37
38
39

40 **2.2. Synthesis of Fe-TNTs.** A modified one-step water-ethanol hydrothermal
41
42 method was used to fabricate Fe-TNTs. First, 1.08 g FeCl₃·6H₂O and 0.48 g NaOH
43
44 were mixed in a beaker with 40 mL absolute ethanol. After stirring under ultrasonic
45
46 conditions for 30 min, 0.6 g TiO₂ (P25), 21 g NaOH, and 25mL deionized water were
47
48 further added. The mixture was then stirred for a further 30 minutes under ultrasonic
49
50 conditions, transferred into a Teflon reactor with stainless steel coating, and heated at
51
52 150 °C for 24 h. Finally, the precipitates were washed with deionized water to neutral,
53
54 and Fe-TNTs were obtained after drying at 80 °C for 6 h.
55
56
57
58
59
60

1
2
3
4 For comparison purposes, conventional TNTs were also synthesized through the
5
6 traditional hydrothermal method described in our previous studies.^{7,30} Typically, 1.2 g
7
8 of TiO₂ (P25) and 29 g of NaOH were mixed and dispersed into 66 mL of deionized
9
10 water. After the mixture was heated in a Teflon reactor at 130 °C for 72 h, the
11
12 products were washed to neutral and dried at 80 °C.
13
14

15
16 **2.3. Photocatalytic Reactions.** Photocatalytic experiments were carried out in a
17
18 quartz reactor (300 mL total volume) (Figure S1 in the Supporting Information), and a
19
20 metallic cover was placed outside to isolate other light sources. 100 mL of As(III)
21
22 solution with an initial concentration of 10 mg L⁻¹ was added into the quartz reactor.
23
24 After the solution pH was adjusted to 3.0 using dilute HCl and NaOH solution,
25
26 0.02–0.06 g of Fe-TNTs were mixed. Before photocatalytic reaction, the mixture was
27
28 stirred in the dark for 4 h to reach equilibrium for As(III) adsorption onto Fe-TNTs.
29
30 Afterwards, a 150 W mercury lamp (365 nm, 2.5 mW cm⁻², Beijing Electric Light
31
32 Sources Research Institute, China) was switched on to start the photocatalysis
33
34 reaction. During the photocatalysis process, cooling air was poured in from the top so
35
36 as to maintain the reaction system at a constant temperature (25 ± 2 °C). Samples
37
38 were taken every 10 min, immediately centrifuged at 10,000 rpm for 2 min,
39
40 and filtered using a 0.22 μm membrane. Photolysis experiments without addition of
41
42 Fe-TNTs were also conducted as control tests. Each set of experiments was performed
43
44 in triplicate.
45
46
47
48
49
50
51
52

53
54 The As(III) photocatalytic reactions are expressed by the classical
55
56 Langmuir-Hinshelwood (L-H) model,²⁹
57
58
59
60

$$-\frac{dC_t}{dt} = r = k_r \frac{K_L C_t}{1 + K_L C_t} \quad (1)$$

where C_t (mg L^{-1}) is the As(III) concentration at time t (min), r ($\text{mg L}^{-1} \text{min}^{-1}$) is the photocatalytic reaction rate, k_r ($\text{mg L}^{-1} \text{min}^{-1}$) is the photocatalytic reaction rate-constant, and K_L (L mg^{-1}) is the Langmuir constant of adsorption. We consider the simplified first-order kinetic model,

$$\ln(C_0 / C_t) = k_1 t \quad (2)$$

where C_0 (mg L^{-1}) is the initial concentration of As(III), and k_1 (min^{-1}) represents the apparent rate constant of reaction ($k_1 = k_r K_L$).

To investigate the removal of As(III) and As(V), experiments were first carried out on the adsorption of these two As ions under different pH values. 50 mL of As solution with an initial concentration of 10 mg L^{-1} was added into an Erlenmeyer flask. After the solution pH was adjusted in the range from 1 to 9, 0.01 g Fe-TNTs were added and the mixture shaken ($25 \text{ }^\circ\text{C}$, 200 rpm) for 6 h. Samples were taken before and after adsorption, and the As concentration immediately measured using atomic fluorescence spectroscopy (AFS-9130, Beijing Jitian, China) after centrifugation and filtration. The adsorption capacity (Q_e , mg g^{-1}) and removal efficiency (R , %) of As at equilibrium are calculated from

$$Q_e = \frac{(C_0 - C_e)V}{m} \quad (3)$$

and

$$R = \frac{(C_0 - C_e)}{C_0} \times 100\% \quad (4)$$

where C_0 (mg L^{-1}) is the initial As concentration, C_e (mg L^{-1}) is the equilibrium As

1
2
3
4 concentration, V (mL) is the solution volume, and m (g) is the mass of Fe-TNTs.
5

6 Photocatalysis experiments at conditions close to real conditions were then
7
8 carried out under visible light irradiation. 10 mg L⁻¹ As(III) was added into a
9
10 quartz reactor at pH 3.0. After addition of 0.02 to 0.06 g Fe-TNTs and an initial 4
11
12 hours' stirring in the dark, a 500 W Xenon arc lamp (470 nm, Beijing Electric Light
13
14 Sources Research Institute, China), which was used in conjunction with UV cutting
15
16 filter ($\lambda \geq 420$ nm), was switched on as the visible light source to start the
17
18 photocatalysis reaction. And the same conditions and procedures were conducted as
19
20 the aforementioned photocatalysis experiments, except for the light source. Samples
21
22 were collected at specific intervals and immediately measured. Control experiments
23
24 were also conducted without addition of Fe-TNTs.
25
26
27
28
29
30

31 **2.4. Reuse of Fe-TNTs.** To evaluate the application potential of Fe-TNTs for
32
33 removal of As(III) and As(V), the material was reused after photocatalysis-adsorption
34
35 experiments under visible light. Specially, a photocatalysis-adsorption test was carried
36
37 out first with initial As(III) concentration of 10 mg L⁻¹ and Fe-TNTs dosage of 0.6 g
38
39 L⁻¹ at pH 3.0. After initial 240 min of adsorption in dark and subsequent 180 min of
40
41 photocatalysis under visible irradiation, materials were separated by centrifugation
42
43 and filtration. Afterwards, the materials were immersed into 100 mL of 1.0 mol L⁻¹
44
45 NaOH solution and shaken for 4 h to desorb As(V). After desorption, Fe-TNTs were
46
47 washed to neutral using DI water, and then reused to remove As under the same
48
49 conditions via photocatalysis and adsorption. Reuse of Fe-TNTs lasted for 5 cycles. In
50
51 addition, the concentration of Fe dissolved into solution in each cycle was detected on
52
53
54
55
56
57
58
59
60

1
2
3
4 an inductively coupled plasma-optical emission spectrometry (ICP-OES, Prodigy,
5
6 Leeman, USA).
7

8
9 **2.5. Analysis of Hydroxyl Radicals.** Formation of hydroxyl radicals ($\cdot\text{OH}$) in
10
11 the photocatalysis reaction was detected by a photoluminescence (PL) technique using
12
13 terephthalic acid as the probe molecule. Terephthalic acid reacted readily with $\cdot\text{OH}$ to
14
15 form a highly fluorescent product, 2-hydroxyterephthalic acid, whose intensity was
16
17 proportional to the amount of $\cdot\text{OH}$ present. A total of 0.01 g of Fe-TNTs was
18
19 dispersed into a mixture of 0.5 mmol terephthalic acid and 2 mmol NaOH occupying
20
21 a total volume of 10 mL in a dish. Afterwards, the mixture was irradiated under UV
22
23 light and samples were taken every 15 min. After filtration, the PL spectra of samples
24
25 were measured by a Hitachi F-4500 fluorescence spectrophotometer with
26
27 photomultiplier tube (PMT) R928. The PL intensity of 2-hydroxyterephthalic acid
28
29 was determined at 425 nm, excited by 320 nm light.
30
31
32
33
34
35

36
37 **2.6. Characterizations.** Morphology of the material was analyzed using a
38
39 Tecnai30 FEG transmission electron microscopy microscope (TEM, FEI, USA)
40
41 operating at 300 kV. Energy dispersive X-ray spectra (EDS) were also recorded. The
42
43 crystal phase of the sample was obtained by means of a Dmax/2400 X-ray
44
45 diffractometer (XRD, Rigaku, Japan) using Cu $K\alpha$ radiation ($\lambda = 1.5418 \text{ \AA}$) at a scan
46
47 rate (2θ) of $4^\circ/\text{min}$. Specific surface areas of the materials were determined via
48
49 nitrogen adsorption-desorption isotherms at -196°C using an ASAP2010 adsorption
50
51 apparatus (Micromeritics, USA) based on Brunauer-Emmett-Teller (BET) theory.
52
53
54
55
56
57 Pore volume and mean pore diameter were measured by means of the nitrogen
58
59
60

1
2
3
4 adsorption volume at a relative pressure of 0.99. Surface functional groups were
5
6 determined using Fourier Transform infrared spectroscopy (FTIR, Tensor 27, Bruker,
7
8 Germany) through the KBr pellet method. Element composition and the oxidation
9
10 state of samples were recorded on an AXIS-Ultra X-ray photoelectron spectroscopy
11
12 (XPS, Kratos, England) using Al $K\alpha$ X-ray source at 15 kV and 15 mA. Standard C 1s
13
14 peak (Binding energy, $E_b = 284.80$ eV) was used to eliminate static charge effects.
15
16
17 The UV-visible spectrum of each sample was recorded by a UV-1800 (Shimadzu,
18
19 Japan) after the material was dispersed in water. Diffuse reflectance (DRS)
20
21 UV-visible adsorption spectra of the materials were obtained using a UV-2400
22
23 spectrophotometer (Shimadzu, Japan). $BaSO_4$ powder was used as reference at all
24
25 energies (100% reflectance) and reflectance measurements were converted to
26
27 adsorption spectra using the Kubelka-Munk function. Zeta potential and size of
28
29 samples were obtained using a Nano-ZS90 Zetasizer (Malvern Instruments, UK).
30
31
32
33
34
35
36

37 3. RESULTS AND DISCUSSION

38
39 **3.1. Characteristics of Fe-TNTs.** The as-synthesized TNTs comprised 4–5
40
41 layers of hollow and open-ended nanotubes, which had uniform interior (ca. 4.5 nm)
42
43 and outer (ca. 9 nm) diameters (Figure S2 in the Supporting Information). The
44
45 interlayer distance was 0.75 nm (Figure S2b in the Supporting Information).³⁰ EDS
46
47 analysis indicated that the main elements in TNTs were Na, O, and Ti (Figure S2c in
48
49 the Supporting Information). After the Fe was deposited, the surface of nanotubes
50
51 became rough, with some nanoparticles attached (Figure 1). The interlayer distance of
52
53 Fe-TNTs increased to 0.78 nm due to entry of Fe^{3+} .⁷ The lattice distance of attached
54
55
56
57
58
59
60

nanoparticles was 0.25 nm (Figure 1b), which was assigned to the (110) plane of Fe_2O_3 (JCPDS 24-0072). An Fe element peak was also observed in the results from EDS analysis (Figure 1c), indicating that Fe had been successfully deposited onto TNTs.

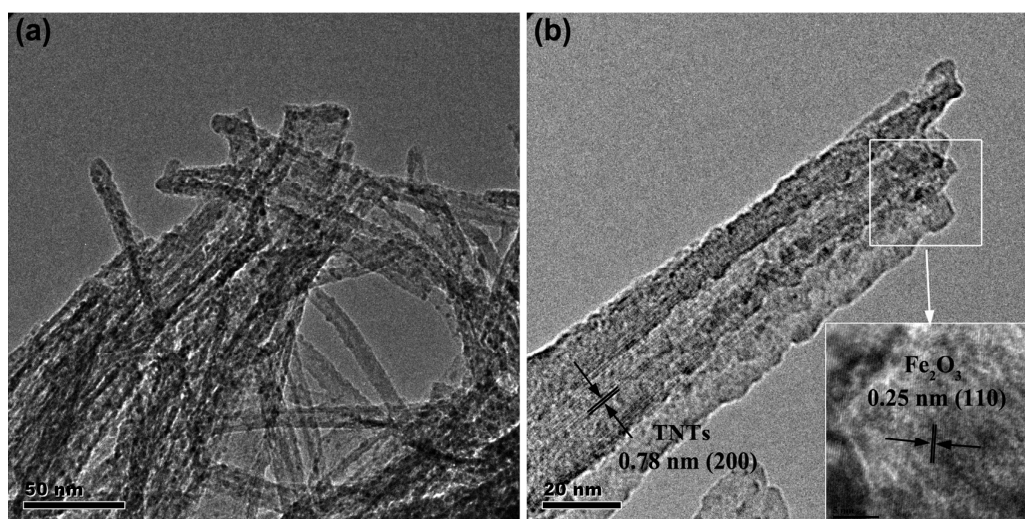


Figure 1. (a) TEM, (b) HRTEM image and (c) EDS spectrum of Fe-TNTs.

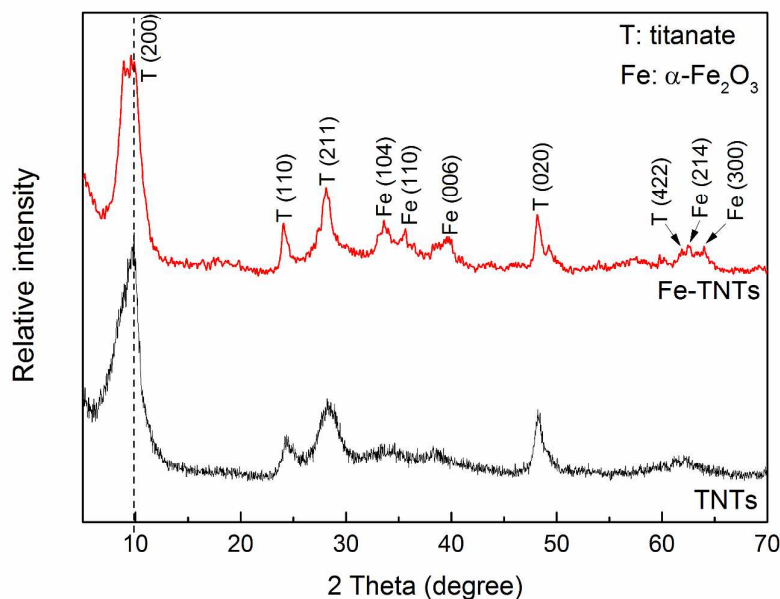


Figure 2. XRD patterns of TNTs and Fe-TNTs.

XRD further confirmed the deposition of Fe (Figure 2). Diffraction peaks at $2\theta \approx 10^\circ, 24^\circ, 28^\circ, 48^\circ$ and 62° were all attributed to TNTs, and in particular, the 10° peak represented the interlayer space of TNTs.^{31, 32} For Fe-TNTs, besides the diffraction of TNTs, the new peaks at $2\theta = 33.6^\circ, 35.6^\circ, 40.0^\circ, 44.7^\circ, 62.5^\circ,$ and 64.0° were consistent with (104), (110), (006), (202), (214), and (300) planes of $\alpha\text{-Fe}_2\text{O}_3$ phases (JCPDS 24-0072). Moreover, the interlayer peak of Fe-TNTs shifted to 9.59° from 9.86° of TNTs, indicating an increase in the interlayer distance (smaller 2θ degree meant larger interlayer distance), related to the entry of Fe^{3+} . Here, the TNTs were a kind of sodium trititanate with the chemical formula of $\text{Na}_x\text{H}_{2-x}\text{Ti}_3\text{O}_7$ ($x = 0\text{--}0.75$, depending on remaining sodium ions), which was composed of edge-sharing $[\text{TiO}_6]$ octahedrons as the basic skeleton and H^+/Na^+ between the layers.³¹⁻³³ Interlayer

1
2
3
4 H^+/Na^+ ions were readily replaced by Fe^{3+} during the hydrothermal process, causing
5
6 the interlayer distance to increase. Deposited Fe in Fe-TNTs therefore existed in two
7
8 forms: $\alpha-Fe_2O_3$ attached on TNTs; and Fe^{3+} located in the interlayers of TNTs.
9

10
11 Figure 3 shows the FTIR spectra obtained for the both the TNTs and Fe-TNTs.
12
13 Considering the spectrum related to the TNTs, the bands at 476 and 925 cm^{-1}
14
15 corresponded respectively to vibration of the $[TiO_6]$ octahedron and four-coordinate
16
17 Ti–O stretching.^{32, 34} After Fe deposition, an additional band appeared at 652 cm^{-1}
18
19 representing Fe–O vibration.³⁵ Bands at 3313 and 1631 cm^{-1} were ascribed to the
20
21 stretching vibrations of O–H and H–O–H, respectively. The shift of the O–H band to
22
23 3395 cm^{-1} for Fe-TNTs was due to the interaction of hydroxyl groups with Fe^{3+} .³⁴ The
24
25 band at 1383 cm^{-1} corresponding to O–Na stretching vibration almost disappeared for
26
27 Fe-TNTs, confirming that the interlayered Na^+ were exchanged by Fe^{3+} .³⁶
28
29
30
31
32
33
34
35

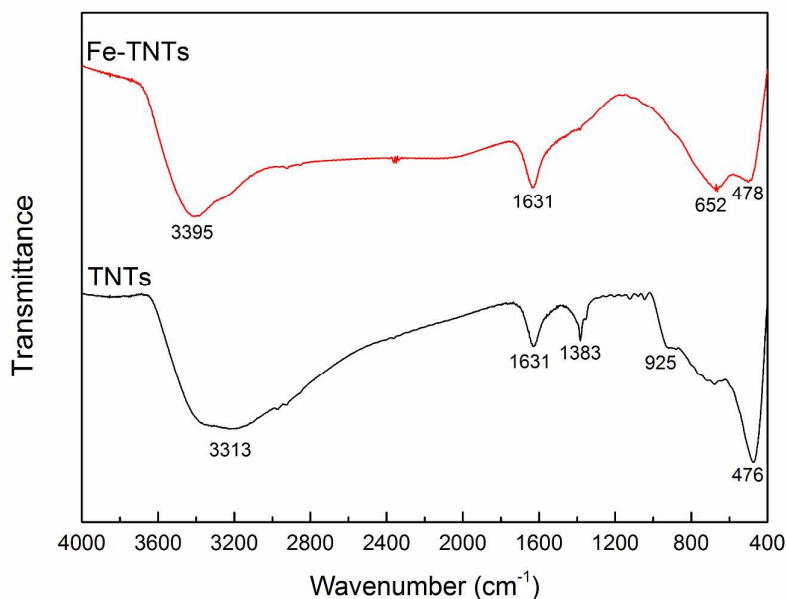


Figure 3. FT-IR spectra of TNTs and Fe-TNTs.

1
2
3
4 Table 1 provides a list of key physiochemical parameters describing the
5
6 unmodified TNTs and Fe-TNTs. The large BET surface area ($162.8 \text{ m}^2 \text{ g}^{-1}$) and single
7
8 point total pore volume ($0.38 \text{ cm}^3 \text{ g}^{-1}$) of the Fe-TNTs benefited both photocatalysis
9
10 and adsorption through enhanced contact with As ions. Moreover, the N_2
11
12 adsorption-desorption isotherms on Fe-TNTs fitted type IV isotherms with H3
13
14 adsorption-desorption isotherms on Fe-TNTs fitted type IV isotherms with H3
15
16 hysteresis loops according to BDDT classification,³⁷ suggesting the presence of
17
18 mesopores (2–50 nm) in Fe-TNTs (Figure S3a in the Supporting Information). The
19
20 pore size of Fe-TNTs exhibited a trimodal distribution, as shown in Figure S3b in the
21
22 Supporting Information. Pores with peak diameters in the range of 3–4 nm, 8–9 nm,
23
24 and 10–20 nm were respectively attributed to the interior of the nanotubes, gaps
25
26 between the Fe_2O_3 nanoparticles and TNTs, and voids in the aggregation of the
27
28 nanotubes.^{38, 39} Attachment of Fe_2O_3 nanoparticles inevitably blocked some pores of
29
30 the TNTs, leading to a decrease in specific surface area and pore volume compared to
31
32 the unmodified TNTs. The point of zero charge (pH_{PZC}) for Fe-TNTs increased to 5.49
33
34 after Fe was deposited, a much higher value than that for unmodified TNTs (2.56)
35
36 (Figure S4 in the Supporting Information), which is benefited to the adsorption of
37
38 metal anions, such as As(V) .^{27, 28}
39
40
41
42
43
44
45
46
47
48
49
50
51
52
53
54
55
56
57
58
59
60

Table 1. Physicochemical parameters of unmodified TNTs and Fe-TNTs.

Material	BET surface area (m ² g ⁻¹)	Single point	Average	pH _{PZC}	Atomic percentage content (%)			
		total volume (cm ³ g ⁻¹)	pore pore diameter (nm)		Na	O	Ti	Fe
Fe-TNTs	162.8	0.38	9.3	5.49	9.1	62.7	21.8	6.4
TNTs	272.3	1.26	18.5	2.56	12.3	64.3	23.4	0.0

3.2. Adsorption of As(III) and As(V) by Fe-TNTs. Figure 4 depicts the adsorption of As(III) and As(V) for different pH values. The adsorption capacity of As(III) on TNTs remained small (< 10 mg g⁻¹) throughout the range of pH considered, and was related to the form of As(III) species in solution. Molecular H₃AsO₃ was the main species of As(III) over a wide pH range (Figure S5a in the Supporting Information) and complexation by hydroxyl groups of Fe-TNTs was the dominant mechanism,²⁷ resulting in an almost unchanged As(III) adsorption capacity. Photocatalysis was therefore necessary to remove As(III), after which the oxidation products, As(V), could be further adsorbed onto Fe-TNTs.

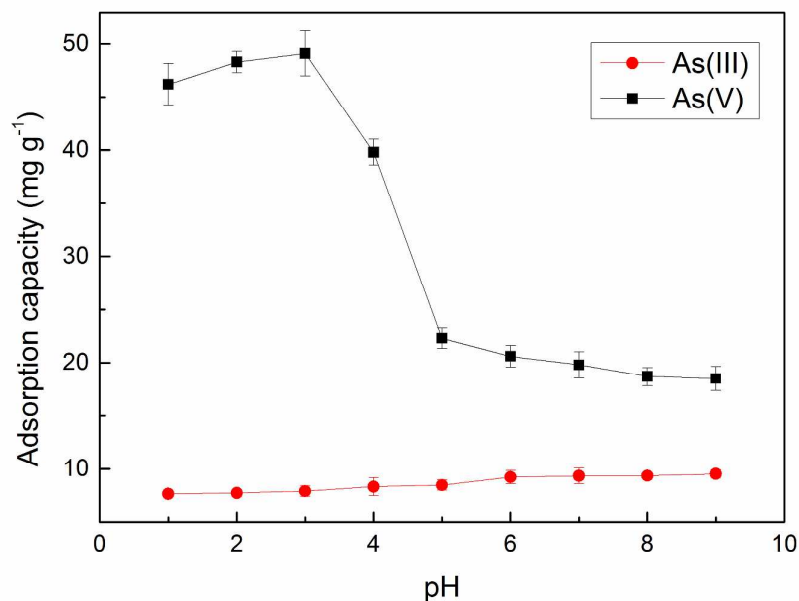


Figure 4. Adsorption of As(III) and As(V) by Fe-TNTs at different pH. (Initial As concentration = 10 mg L⁻¹; Fe-TNTs dosage = 0.2 g L⁻¹.)

The adsorption was extremely different for As(V) adsorption onto Fe-TNTs as a function of pH. Fe-TNTs exhibited good adsorption performance for As(V), especially at low pH (2 and 3). For instance, the adsorption capacity of As(V) reached 49.1 mg g⁻¹ at pH 3, with a correspondingly high removal efficiency of 98.2%. Fe-TNTs were positively charged at low pH (Figure S4 in the Supporting Information), and thus could capture As(V) anions (H₂AsO₄⁻) through electrostatic attraction (Figure S5b in the Supporting Information). Moreover, As(V) in the main form of molecular H₃AsO₄ was hardly attracted to Fe-TNTs at pH 1, even though the Fe-TNTs had their highest positive charge at low pH. As the pH further increased (> 3), the amount of positive charge decreased (Figure S4 in the Supporting Information), thus lowering the As(V)

1
2
3
4 adsorption capacity. Moreover, increased OH^- at higher pH would compete for
5
6 adsorption sites with As(V) anions, further lowering the adsorption capacity.^{27, 28, 34}
7
8
9 Noting the high adsorption efficiency of As(V) , a pH value of 3 was chosen for the
10
11 following photocatalysis-adsorption experiments.
12

13
14 **3.3. Photocatalysis of As(III) by Fe-TNTs under UV Light.** Figure 5 presents
15
16 time histories of As(III) and As(V) concentrations, each for three initial dosage
17
18 values, throughout the photocatalysis-adsorption process under UV light. Before the
19
20 light was switched on (from $t = -240$ to 0 min), a portion of As(III) was removed in
21
22 the dark by adsorption on the Fe-TNTs. During this phase, the adsorption capacity of
23
24 As(III) onto Fe-TNTs was limited, given that there was still 59.6% As(III) remaining
25
26 even at a high Fe-TNTs dosage of 0.6 g L^{-1} . In addition, adsorption of As(III) could
27
28 reach to equilibrium with 180 min (Figure S6 in the Supporting Information), so 240
29
30 min is enough for As(III) adsorption in this study. Once the light was switched on, the
31
32 removal of As(III) was primarily due to photocatalysis (for $t = 0$ to 120 min), and the
33
34 total removal efficiency exceeded 99% after 70 min for all three initial dosages
35
36 considered. Notably, 99.6% of As(III) of initial dosage 0.6 g L^{-1} was photo-oxidized
37
38 within 30 min, indicating the extremely high photocatalytic ability of Fe-TNTs. Table
39
40 2 lists the parameters of the first-order kinetic model for As(III) under photocatalysis
41
42 by Fe-TNTs. The higher was the initial dosage of Fe-TNTs, the larger the value of
43
44 apparent rate constant (k_1). Very weak photocatalytic performance for As(III)
45
46 oxidation was found for TNTs (Figure S7 in the Supporting Information).
47
48 Comparatively, the k_1 value for photo-oxidation of As(III) by Fe-TNTs (0.1512 min^{-1})
49
50
51
52
53
54
55
56
57
58
59
60

was almost 250 times of that by unmodified TNTs (0.0006 min^{-1}) at the same initial dosage of 0.6 g L^{-1} , suggesting Fe played an important role and Fe deposition substantially enhanced the photocatalytic activity of TNTs.

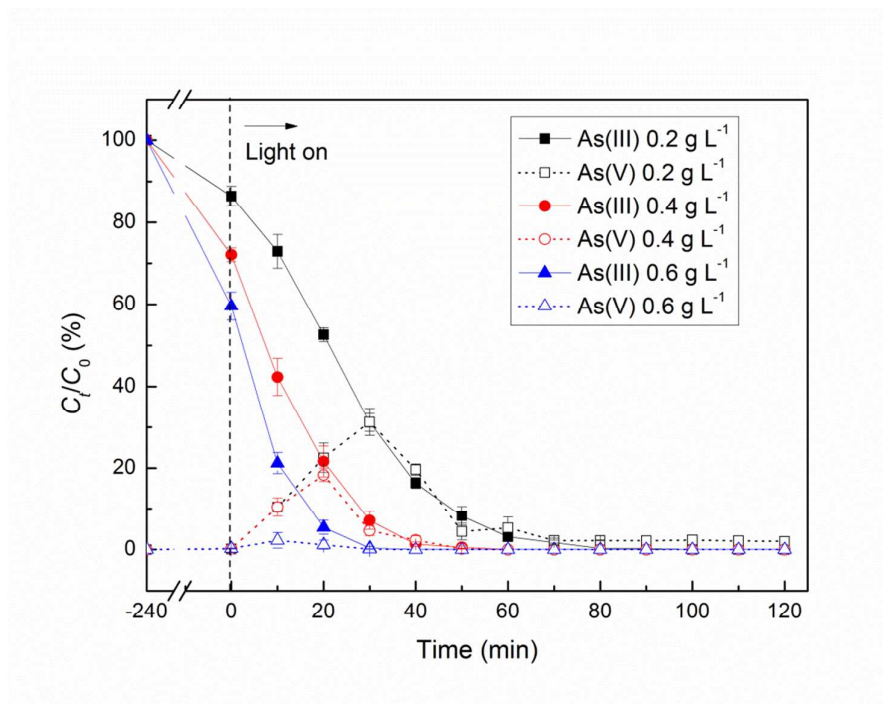


Figure 5. Photocatalysis-adsorption of As(III) and As(V) by Fe-TNTs at different initial dosages under UV light. (Initial As(III) concentration = 10 mg L^{-1} ; solution pH = 3.0).

Table 2. Parameters of first-order kinetic model for As(III) photocatalysis by Fe-TNTs.

Dosage (g L ⁻¹)	UV light		Visible light	
	<i>k</i> ₁ (min ⁻¹)	<i>R</i> ²	<i>k</i> ₁ (min ⁻¹)	<i>R</i> ²
0.2	0.0596	0.9195	0.0086	0.9965
0.4	0.0917	0.9506	0.0173	0.9915
0.6	0.1512	0.9356	0.0263	0.9886

For As(V) removal, the ratio C_t/C_0 in Figure 5 is equivalent to the conversion efficiency from As(III) to As(V), as the value of C_0 was 10 mg L⁻¹ (if total conversion). The process involved simultaneous production and elimination of As(V). On the one hand, As(III) was photo-oxidized to As(V) which then accumulated in solution. On the other hand, the produced As(V) was continuously adsorbed onto Fe-TNTs, and Figure S6 in the Supporting Information indicates that adsorption of As(V) could reach to equilibrium within 300 min while mainly occurred in the first 90 min. Therefore, the As(V) concentration initially increased to a peak value before declining to about zero. At high (0.6 g L⁻¹) initial dosage Fe-TNTs almost no As(V) was detected over the entire photocatalysis-adsorption process, indicating that the abundant adsorption sites simultaneously adsorbed all the produced As(V). Therefore, a combination of photocatalysis and adsorption on Fe-TNTs led to the efficient removal of As(III) and As(V), thus achieving the goal of complete removal of As.

3.4. Removal of As(III) and As(V) by Fe-TNTs under Visible Light. Figure 6 shows the corresponding results to those in Figure 5, except that visible light is used

1
2
3 instead of UV as the light source. From the time histories in Figure 6, it can be seen
4
5 that As(III) was also efficiently oxidized to As(V) under visible light, although the
6
7 photocatalytic reactions required more time than those under UV irradiation (Figure
8
9 5). The removal efficiency of As(III) reached 99.6% at 300 min for an initial dosage
10
11 of 0.4 g L⁻¹ Fe-TNTs and 99.5% at 180 min for an initial dosage of 0.6 g L⁻¹ Fe-TNTs,
12
13 indicating good photocatalytic performance even under visible light. Although some
14
15 As(III) converted to As(V) through photolysis and photocatalysis by unmodified
16
17 TNTs (Figure S8 in the Supporting Information), the conversion efficiency was
18
19 relatively low (8% and 9.6% respectively within 360 min). This indicates that
20
21 oxidation of As(III) under visible light greatly enhanced by Fe-TNTs due to Fe
22
23 deposition, and the mechanism will be detailly discussed later. Furthermore, only
24
25 trace amounts of As(V) accumulated in solution (< 2%) over the entire
26
27 photocatalysis-adsorption process. The photocatalytic rate of As(III) oxidation
28
29 decreased after UV light was replaced by visible light, but the adsorption rate of
30
31 As(V) was unaffected, resulting in immediate uptake of As(V). The high
32
33 photocatalytic activity of Fe-TNTs under visible light is of great importance for future
34
35 applications in environmental remediation. Considering the excellent removal
36
37 efficiency of As(III) and As(V) at 0.6 g L⁻¹ of Fe-TNTs, this optimum dosage was
38
39 chosen for the further reusability tests.
40
41
42
43
44
45
46
47
48
49
50
51
52
53
54
55
56
57
58
59
60

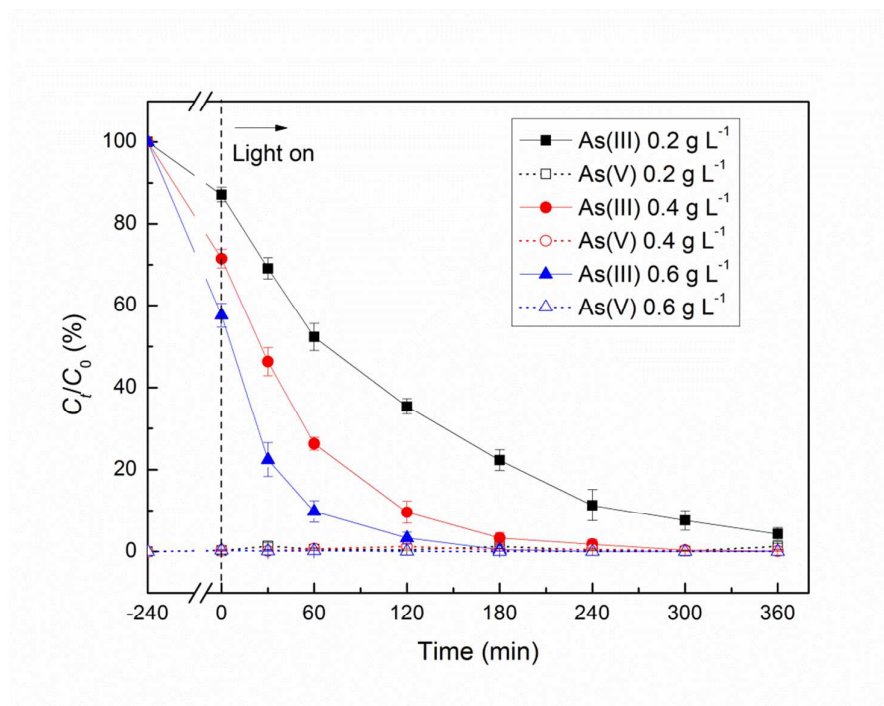


Figure 6. Photocatalysis-adsorption of As(III) and As(V) by Fe-TNTs at different initial dosages under visible light (Initial As(III) concentration = 10 mg L^{-1} ; solution pH = 3.0).

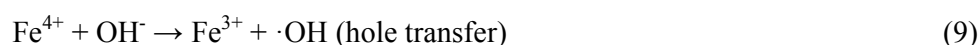
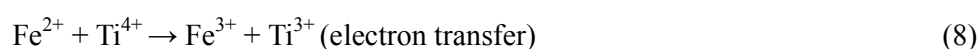
3.5. Enhancement Mechanisms of Photocatalytic Activity and Adsorptive Property.

3.5.1. Role of Deposited Fe on Enhancement of Photocatalytic Activity. The preceding results show that the photocatalytic activity of TNTs was greatly enhanced by deposited Fe. For TNTs, the electron-hole pairs easily recombined after excitation through irradiation, leading to extremely low photocatalytic activity.^{3, 10} The deposited Fe existed in two forms in Fe-TNTs, i.e. interlayered Fe^{3+} and $\alpha\text{-Fe}_2\text{O}_3$, resulting in dual enhancement of photocatalytic activity. Firstly, the Fe^{3+} in the interlayers of TNTs could act as a temporary electron (e^-) or hole (h^+) trapping site

that inhibited recombination,⁴⁰ through the following processes:

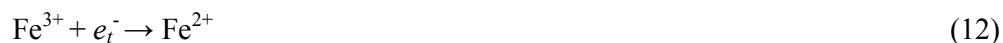
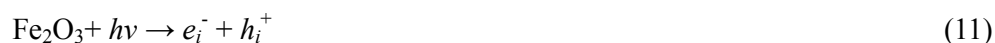


Due to the instability of Fe^{2+} and Fe^{4+} , transfer of trapped charges from Fe^{4+} and Fe^{2+} to Fe^{3+} also occurred in the titanate surface as follows:



Secondly, $\alpha\text{-Fe}_2\text{O}_3$ could also generate an electron-hole pair under irradiation, and therefore act as a charge carrier for electrons transferred from TNTs. The TEM and XRD analyses showed the close coupling between TNTs and $\alpha\text{-Fe}_2\text{O}_3$, which meant that an excited electron from TNTs with a lower conduction band could recombine with a hole in Fe_2O_3 , thus inhibiting recombination of electron-hole pairs of TNTs.⁴¹

The processes are summarized as follows:



During photocatalysis, As(III) oxidation involved the following reactions:⁴²



14
15
16
17
18
19
20
21
22
23
24
25
26
27
28
29
30
31
32
33
34
35
36
37
38
39
40
41
42
43
44
45
46
47
48
49
50
51
52
53
54
55
56
57
58
59
60

As illustrated by the UV-vis spectra (DRS) (Figure 7), the TNTs exhibited an adsorption edge of 361 nm, whereas Fe deposition led to a dramatic red shift into the visible range of 499 nm. For Fe-TNTs, the peak at ca. 480 nm was related to intrinsic absorption of Fe(III). Using the Kubelka-Munk method,⁴³ the band gap energy (E_g) of the Fe-TNTs was determined as 2.5 eV, a much lower value than that of the unmodified TNTs (3.4 eV). After Fe was deposited, the Fe 3d electron energy levels were higher than those of Ti 3d, leading to the levels emerging in the gap region between the O 2p and Ti 3d dominant bands.⁴⁴ The red shift to visible region in the UV-vis spectra (DRS) of Fe-TNT implies this is a promising candidate for solar energy applications under visible light, as confirmed in Figure 6. Although previous studies confirmed the calcination and acid treatment can enhance the photocatalytic activity of TNTs under UV light, while no visible light can be adsorbed and used by these TNTs materials (calcined and hydrogen TNTs) for photocatalysis.^{4, 10, 13, 14}

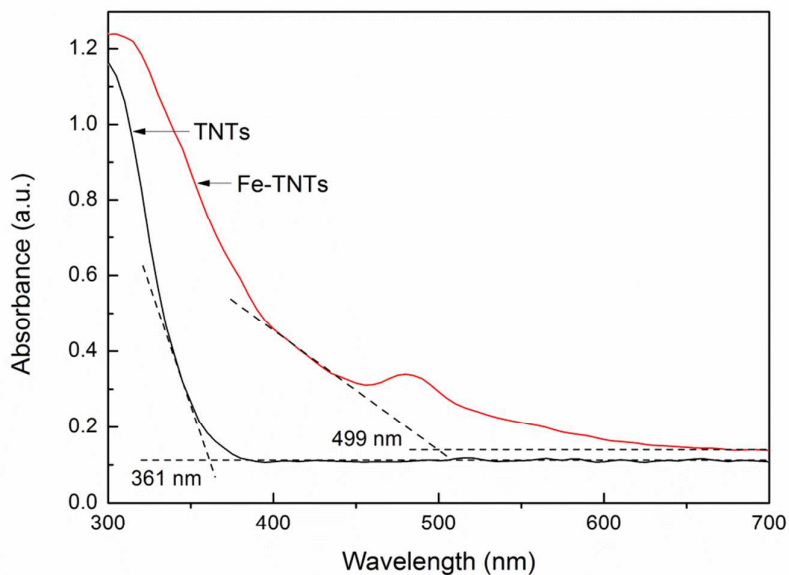


Figure 7. UV-vis spectra (DRS) of TNTs and Fe-TNTs.

PL spectra of terephthalic acid reflected the formation of $\cdot\text{OH}$ under UV irradiation in the presence of Fe-TNTs (Figure 8). It can be seen that the fluorescence intensity amplified with increasing irradiation time, indicating growth in the amount of $\cdot\text{OH}$ in the presence of Fe-TNTs. However, almost no $\cdot\text{OH}$ formed when TNTs were used as the photocatalyst (Figure S9 in the Supporting Information), again implying that Fe deposition greatly enhanced photocatalytic activity.

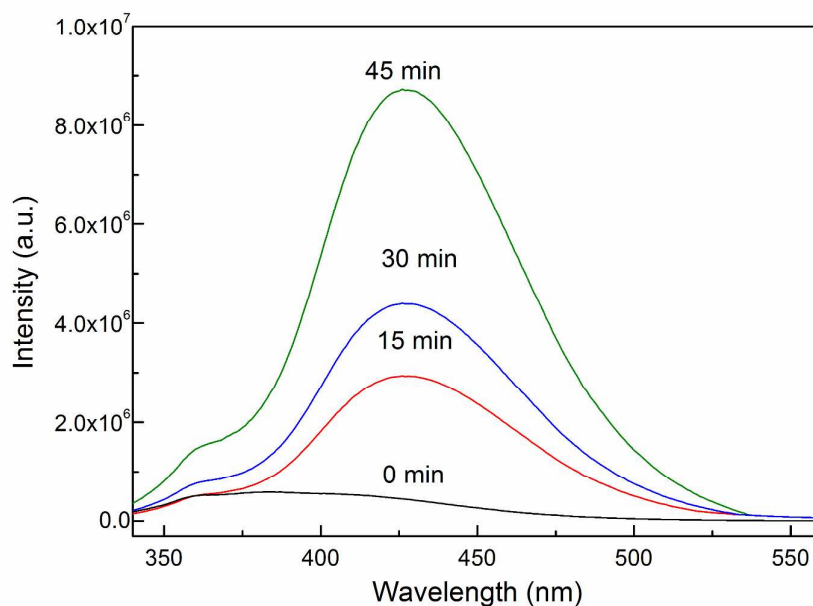


Figure 8. PL spectra for terephthalic acid in the presence of Fe-TNTs as a function of irradiation time.

3.5.2. Role of Deposited Fe on Enhancement of Adsorptive Property. Fe-TNTs also exhibited an excellent adsorptive property for As(V). According to the two-site Langmuir isotherm model (Supporting Information), the maximum adsorption capacity of As(V) on Fe-TNTs was found to be 88.72 mg g^{-1} , a much larger value than that for the unmodified TNTs of 27.54 mg g^{-1} (Table S1 in the Supporting Information). Two contributory reasons for this enhancement of the adsorptive property are: (1) an increase in the pH_{PZC} -induced efficient capture of As(V) anions through electrostatic attraction; and (2) the deposited $\alpha\text{-Fe}_2\text{O}_3$ could also adsorb As(V) through surface hydroxyl groups. It is relevant to note the two kinds of adsorption sites in Fe-TNTs, i.e. TNTs and $\alpha\text{-Fe}_2\text{O}_3$ (Supporting Information). Therefore, the critical

problem on small adsorption capacity of TNTs for the metal anion, As(V), is also solved by Fe-TNTs due to Fe deposition, which is the basis for simultaneous removal of both As(III) and As(V).

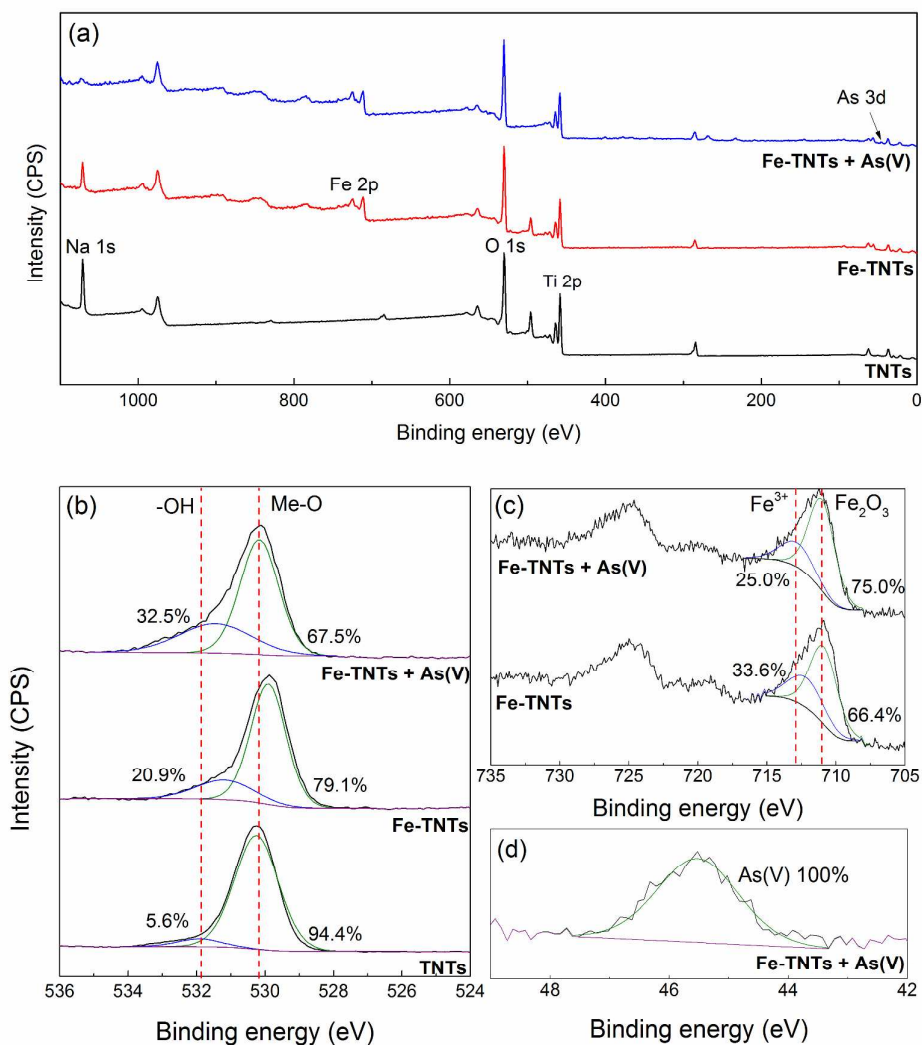


Figure 9. XPS spectra for TNTs, Fe-TNTs, and Fe-TNTs with As (V): (a) survey and high resolution spectra of (b) O 1s, (c) Fe 2p and (d) As 3d.

The adsorption process of As(V) comprised initial electrostatic attraction and subsequent complexation. This is further illustrated by the results of the XPS analysis in Figure 9, which showed that the main component elements of TNTs were Na, O

1
2
3 and Ti (Figure 9a). After the Fe was deposited, the Fe 3d peak emerged and the atomic
4 percentage of Fe on Fe-TNTs was 6.4% (Table 1), in accordance with the EDS spectra
5
6
7
8
9 (Figure 1c). The atomic percentage of Na in Fe-TNTs decreased to 9.1% compared to
10
11 12.3% in TNTs, owing to the ion-exchange of Fe^{3+} with Na^+ in the interlayers. An As
12
13 3d peak appeared after adsorption, indicating the successful combination of As(V) by
14
15 Fe-TNTs. Figure 9b shows a high resolution spectral view in the vicinity of O 1s;
16
17 the peaks at ca. 532 and 530 eV were respectively attributed to O bonded with metals
18
19 (Me–O) and from hydroxyl groups (–OH).⁴⁵ The composition percentage of –OH for
20
21 Fe-TNTs (20.9%) was higher than that for TNTs (5.6%), due to the presence of large
22
23 hydroxyl groups attached to the $\alpha\text{-Fe}_2\text{O}_3$ surface. It has previously been established
24
25 that –OH groups play a major role in As(V) adsorption, with complexation the
26
27 adsorption mechanism.⁴⁶⁻⁴⁸ Figure S10 in the Supporting Information illustrates the
28
29 difference between the two main complexation processes: bidentate complexation
30
31 does not introduce –OH groups whereas monodentate complexation replaces a single
32
33 –OH by two –OH groups from As(V). For adsorption of As(V) by Fe-TNTs, the –OH
34
35 percent further increased to 32.5% after adsorption, suggesting monodentate
36
37 complexation of As(V) must have occurred in the adsorption process. The peaks at ca.
38
39 711 and 725 eV in the high resolution profile of Fe corresponded to 2p 3/2 and 2p 1/2
40
41 of oxidized iron (Figure 9c).^{49,50} In particular, the 2p 3/2 peak related to Fe(III) from
42
43 $\alpha\text{-Fe}_2\text{O}_3$ (ca. 711 eV) and located in the interlayers (Ti–O–Fe, ca. 713 eV).⁴⁹ The
44
45 slight decrease in amplitude of Ti–O–Fe peak after adsorption was due to H^+
46
47 replacing part of the interlayered Fe^{3+} under acid conditions (pH 3 for the adsorption
48
49
50
51
52
53
54
55
56
57
58
59
60

experiment). The high resolution view shows that the adsorbed As was entirely composed of As(V) (Figure 9d), suggesting full conversion of As(III) during photocatalysis.

3.5.3 Mechanisms for Simultaneous Photocatalysis of As(III) and Adsorption of As(V) by Fe-TNTs. Figure 10 depicts schematically the photocatalysis and adsorption processes for co-removal of As(III) and As(V) by Fe-TNTs. Deposited Fe greatly increases the photocatalytic activity of TNTs, leading to a dual-enhancement effect on arsenic removal. The interlayered Fe^{3+} acts as a temporary electron or hole trapping site, while loaded $\alpha\text{-Fe}_2\text{O}_3$ helps transfer electrons created by the TNTs, both of which mechanisms inhibit the electron-hole pair recombination of TNTs. In addition, reactive oxygen species ($\cdot\text{OH}$ and $\cdot\text{O}_2^-$) form during the conversion process of $\text{Fe}^{4+}/\text{Fe}^{2+}$ to Fe^{3+} , which then oxidize As(III) to As(V). Afterwards, As(V) can be efficiently adsorbed onto Fe-TNTs through complexation.

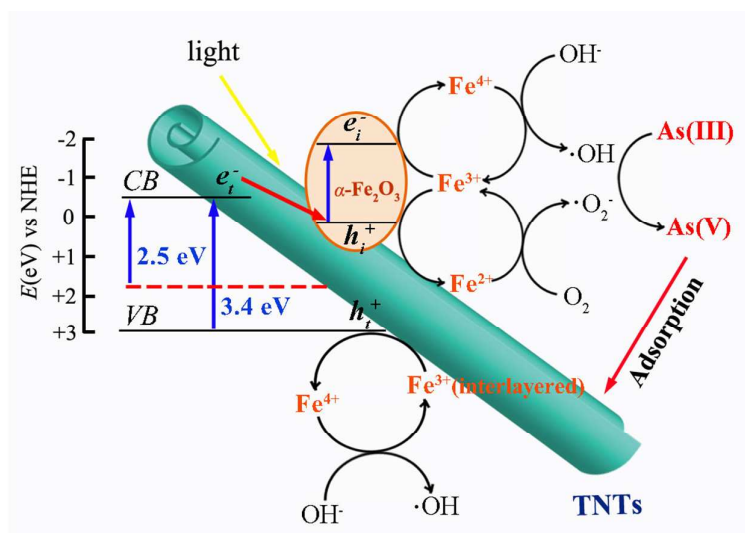


Figure 10. Schematic diagram of the photocatalysis of As(III) and adsorption of As(V) on Fe-TNTs.

1
2
3
4 In conclusion, Fe is an ideal element by which to modify TNTs so as to achieve
5
6 simultaneous removal of As(III) and As(V). The synthesized Fe-TNTs are different
7
8 from the conventional sodium and hydrogen TNTs considering its powerful properties
9
10 on photocatalysis and adsorption. On one hand, deposition of Fe significantly
11
12 enhances photocatalytic performance, especially under visible light. On the other hand,
13
14 deposited iron oxide has excellent adsorptive characteristics and so is ideal for As(V)
15
16 removal. A practicable technology for arsenic removal is first to modify TNTs using
17
18 Fe via a one-step hydrothermal method, and then to use the synthesized Fe-TNTs to
19
20 remove simultaneously As(III) and As(V) through a photocatalysis-adsorption
21
22 process.
23
24
25
26
27

28
29 **3.6. Reuse of Fe-TNTs for As(III) and As(V) Removal.** Fe-TNTs was reused
30
31 after desorption for removal of As(III) and As(V) under visible light via 5 cycles
32
33 (Figure 11). The desorption rate of As(V) from Fe-TNTs was > 99% in each cycle
34
35 with 1.0 mol L⁻¹ NaOH solution treatment. It is found that even after 5 continuous
36
37 photocatalysis-adsorption cycles, the final removal efficiency of As(III) and As(V)
38
39 could reach up to 97.8% and 99.8%, respectively, suggesting good reusability of
40
41 Fe-TNTs. Moreover, only a total amount of 4.3% of Fe dissolved into solutions from
42
43 Fe-TNTs after 5 cycles, indicating the great stability of this material. Therefore,
44
45 Fe-TNTs are of great potential for As removal in practical wastewaters.
46
47
48
49
50
51
52
53
54
55
56
57
58
59
60

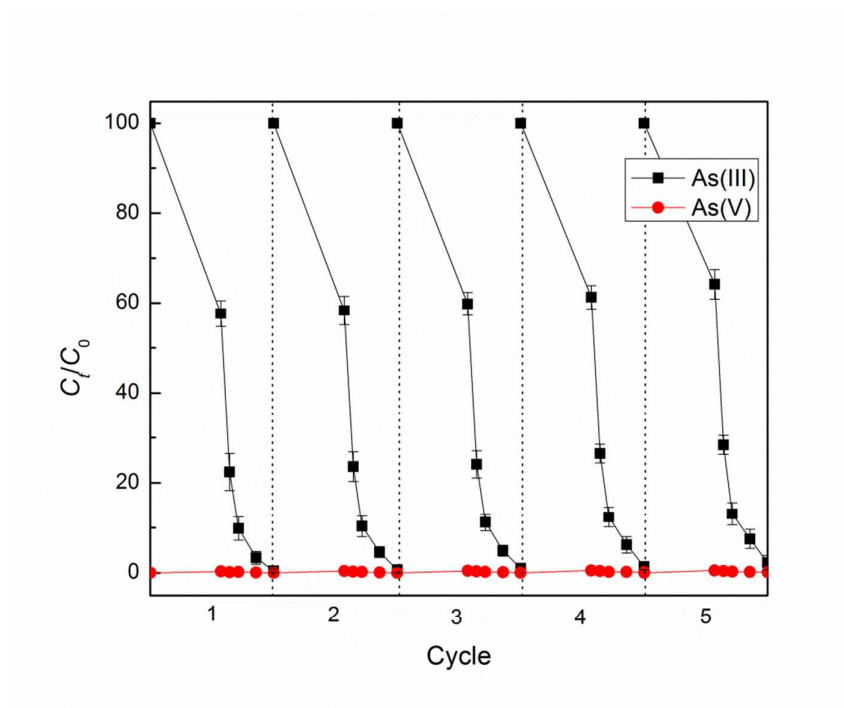


Figure 11. Reuse of Fe-TNTs for As(III) and As(V) removal over 5 photocatalysis-adsorption cycles under visible light (Initial As(III) concentration = 10 mg L⁻¹; material dosage = 0.6 g L⁻¹; solution pH = 3.0).

4. CONCLUSIONS

Fe-deposited titanate nanotubes (Fe-TNTs) were synthesized through a one-step hydrothermal method. The as-prepared material possessed a tubular structure, with Fe₂O₃ nanoparticles attached to the tubes. XRD and XPS analyses showed that the deposited Fe existed in two forms: Fe³⁺ located in the interlayers of TNTs and α -Fe₂O₃ attached on the nanotubes. The optimum material dosage for As(III) and As(V) removal was found to be 0.6 g L⁻¹ both under UV and visible light. The As(III) removal efficiency reached 99.6% within 30 min for an initial dosage of 0.6 g L⁻¹ Fe-TNTs under UV light irradiation. The apparent rate constant for photo-oxidation of

1
2
3
4 As(III) by Fe-TNTs (0.1512 min^{-1}) was almost 250 times that by unmodified TNTs,
5
6 indicating significant enhancement of photocatalytic activity after the Fe was
7
8 deposited. In addition, As(V) was immediately adsorbed onto Fe-TNTs and almost no
9
10 As(V) could be detected throughout the entire photocatalysis-adsorption process.
11
12 Excellent photocatalytic activity was also found under visible light irradiation, with
13
14 99.5% of As(III) photo-oxidized within 180 min for an initial dosage of 0.6 g L^{-1}
15
16 Fe-TNTs. Dual-enhancement of photocatalytic activity occurred after Fe was
17
18 deposited for the following reasons: (1) interlayered Fe^{3+} acted as a temporary
19
20 electron or hole trapping site; (2) $\alpha\text{-Fe}_2\text{O}_3$ acted as a charge carrier for electron
21
22 transferred from TNTs. Both led to inhibited electron-hole pair recombination.
23
24 Moreover, the adsorptive performance of Fe-TNTs was also improved due to the
25
26 presence of attached $\alpha\text{-Fe}_2\text{O}_3$, resulting in efficient removal of As(V) through
27
28 complexation. Initial photocatalysis of As(III) and subsequent adsorption of As(V)
29
30 indicated the key role played by Fe used to modify TNTs. Fe is an ideal metal for
31
32 TNTs modification so as to greatly enhance the photocatalytic and adsorptive property
33
34 of conventional TNTs, thus achieved the goal of simultaneous removal of As(III) and
35
36 As(V).
37
38
39
40
41
42
43
44
45
46

47 ASSOCIATED CONTENT

49 Supporting Information

50 Supporting Information Available: TEM, BET surface area, pore size distribution and
51
52 pH_{PZC} of TNTs; Species distributions of As(III) and As(V); Photo-oxidation of As(III)
53
54 by TNTs under UV and visible light; PL spectra of terephthalic acid in the presence of
55
56
57
58
59
60

1
2
3
4 TNTs; Adsorption kinetics of As(III) and As(V) by Fe-TNTs; Adsorption isotherm and
5
6 mechanism of As(V) by TNTs and Fe-TNTs. This material is available free of charge
7
8 via the Internet at <http://pubs.acs.org>.
9

10 11 12 **AUTHOR INFORMATION**

13 14 **Corresponding Author**

15 *E-mail: nijinren@iee.pku.edu.cn (J.R. Ni), Tel: +86-10-6275-1185;

16
17
18 Fax: +86-10-6275-6526
19

20 21 22 **ACKNOWLEDGMENTS**

23
24 Financial support from National Natural Science Foundation of China (Grant
25
26 No.51379010) is very much appreciated. Supports from U.S. Department of the
27
28 Interior Bureau of Ocean Energy Management (M12AC00013) and Collaborative
29
30 Innovation Center for Regional Environmental Quality of China are also
31
32 acknowledged.
33
34
35

36 37 **REFERENCES**

- 38 1. Pelaez, M.; Nolan, N. T.; Pillai, S. C.; Seery, M. K.; Falaras, P.; Kontos, A. G.; Dunlop, P. S.
39 M.; Hamilton, J. W. J.; Byrne, J. A.; O'Shea, K.; Entezari, M. H.; Dionysiou, D. D. A Review
40 on the Visible Light Active Titanium Dioxide Photocatalysts for Environmental Applications.
41 *Appl. Catal. B: Environ.* **2012**, *125*, 331-349.
- 42 2. Bavykin, D. V.; Friedrich, J. M.; Walsh, F. C. Protonated Titanates and TiO₂ Nanostructured
43 Materials: Synthesis, Properties, and Applications. *Adv. Mater.* **2006**, *18*, 2807-2824.
- 44 3. Kim, S.; Kim, M.; Hwang, S. H.; Lim, S. K. Enhancement of Photocatalytic Activity of
45 Titania-Titanate Nanotubes by Surface Modification. *Appl. Catal. B: Environ.* **2012**, *123-124*,
46 391-397.
- 47 4. Liu, W.; Borthwick, A. G. L.; Li, X.; Ni, J. High Photocatalytic and Adsorptive Performance
48 of Anatase-Covered Titanate Nanotubes Prepared by Wet Chemical Reaction. *Micropor.*
49
50
51
52
53
54
55
56
57
58
59
60

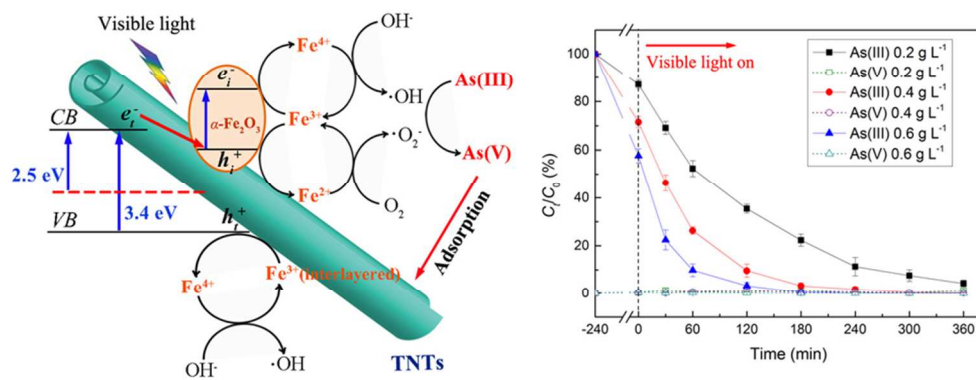
- 1
2
3
4
5
6
7
8
9
10
11
12
13
14
15
16
17
18
19
20
21
22
23
24
25
26
27
28
29
30
31
32
33
34
35
36
37
38
39
40
41
42
43
44
45
46
47
48
49
50
51
52
53
54
55
56
57
58
59
60
- Mesopor. Mater.* **2014**, *186*, 168-175.
5. Weng, B.; Liu, S.; Tang, Z. R.; Xu, Y. J. One-Dimensional Nanostructure Based Materials for Versatile Photocatalytic Applications. *RSC Adv.* **2014**, *4*, 12685-12700.
6. Liu, S.; Tang, Z. R.; Sun, Y.; Colmenares, J. C.; Xu, Y. J. One-Dimension-Based Spatially Ordered Architectures for Solar Energy Conversion. *Chem. Soc. Rev.* **2015**, *44*, 5053-5075.
7. Liu, W.; Wang, T.; Borthwick, A. G. L.; Wang, Y.; Yin, X.; Li, X.; Ni, J. Adsorption of Pb²⁺, Cd²⁺, Cu²⁺ and Cr³⁺ onto Titanate Nanotubes: Competition and Effect of Inorganic Ions. *Sci. Total. Environ.* **2013**, *456-457*, 171-180.
8. Li, N.; Zhang, L.; Chen, Y.; Fang, M.; Zhang, J.; Wang, H. Highly Efficient, Irreversible and Selective Ion Exchange Property of Layered Titanate Nanostructures. *Adv. Funct. Mater.* **2012**, *22*, 835-841.
9. Lin, C. H.; Wong, D. S. H.; Lu, S. Y. Layered Protonated Titanate Nanosheets Synthesized with a Simple One-Step, Low-Temperature, Urea-Modulated Method as an Effective Pollutant Adsorbent. *ACS Appl. Mater. Interfaces* **2014**, *6*, 16669-16678.
10. Lee, C. K.; Wang, C. C.; Lyu, M. D.; Juang, L. C.; Liu, S. S.; Hung, S. H. Effects of Sodium Content and Calcination Temperature on the Morphology, Structure and Photocatalytic Activity of Nanotubular Titanates. *J. Colloid Interface Sci.* **2007**, *316*, 562-569.
11. Yu, H.; Yu, J.; Cheng, B.; Zhou, M. Effects of Hydrothermal Post-Treatment on Microstructures and Morphology of Titanate Nanoribbons. *J. Solid State Chem.* **2006**, *179*, 349-354.
12. Tang, Z. R.; Zhang, Y. H.; Xu, Y. J. Tuning the Optical Property and Photocatalytic Performance of Titanate Nanotube toward Selective Oxidation of Alcohols under Ambient Conditions. *ACS Appl. Mater. Interfaces* **2012**, *4*, 1512-1520.
13. Bavykin, D. V.; Kulak, A. N.; Shvalagin, V. V.; Andryushina, N. S.; Stroyuk, O. L. Photocatalytic Properties of Rutile Nanoparticles Obtained via Low Temperature Route from Titanate Nanotubes. *J. Photoch. Photobio. A: Chem.* **2011**, *218*, 231-238.
14. Yu, J.; Yu, H.; Cheng, B.; Trapalis, C. Effects of Calcination Temperature on the Microstructures and Photocatalytic Activity of Titanate Nanotubes. *J. Mol. Catal. A: Chem.* **2006**, *249*, 135-142.
15. Chen, H. Y.; Lo, S. L.; Ou, H. H. Catalytic Hydrogenation of Nitrate on Cu-Pd Supported on

- 1
2
3 Titanate Nanotube and the Experiment After Aging, Sulfide Fouling and Regeneration
4 Procedures. *Appl. Catal. B: Environ.* **2013**, *142-143*, 65-71.
5
6
7 16. Grandcolas, M.; Cottineau, T.; Louvet, A.; Keller, N.; Keller, V. Solar Light-Activated
8 Photocatalytic Degradation of Gas Phase Diethylsulfide on WO₃-Modified TiO₂ Nanotubes.
9 *Appl. Catal. B: Environ.* **2013**, *138-139*, 128-140.
10
11
12 17. Gannoun, C.; Turki, A.; Kochkar, H.; Delaigle, R.; Eloy, P.; Ghorbel, A.; Gaigneaux, E. M.
13 Elaboration and Characterization of Sulfated and Unsulfated V₂O₅/TiO₂ Nanotubes Catalysts
14 for Chlorobenzene Total Oxidation. *Appl. Catal. B: Environ.* **2014**, *147*, 58-64.
15
16
17 18. Grover, I. S.; Singh, S.; Pal, B., Influence of Thermal Treatment and Au-Loading on the
18 Growth of Versatile Crystal Phase Composition and Photocatalytic Activity of Sodium
19 Titanate Nanotubes. *RSC Adv.* **2014**, *4*, 51342-51348.
20
21
22 19. Choong, T. S. Y.; Chuah, T. G.; Robiah, Y.; Gregory Koay, F. L.; Azni, I. Arsenic Toxicity,
23 Health Hazards and Removal Techniques from Water: An Overview. *Desalination* **2007**, *217*,
24 139-166.
25
26
27 20. Hughes, M. F. Arsenic Toxicity and Potential Mechanisms of Action. *Toxicol. Lett.* **2002**, *133*,
28 1-16.
29
30
31 21. Straif, K.; Benbrahim-Tallaa, L.; Baan, R.; Grosse, Y.; Secretan, B.; El Ghissassi, F.; Bouvard,
32 V.; Guha, N.; Freeman, C.; Galichet, L.; Cogliano, V. A Review of Human Carcinogens-Part
33 C: Metals, Arsenic, Dusts, and Fibres. *Lancet Oncol.* **2009**, *10*, 453-454.
34
35
36 22. Cullen, W. R.; Reimer, K. J. Arsenic Speciation in the Environment. *Chem. Rev.* **1989**, *89*,
37 713-764.
38
39
40 23. Manning, B. A.; Fendorf, S. E.; Bostick, B.; Suarez, D. L. Arsenic(III) Oxidation and
41 Arsenic(V) Adsorption Reactions on Synthetic Birnessite. *Environ. Sci. Technol.* **2002**, *36*,
42 976-981.
43
44
45 24. Zhao, Z.; Jia, Y.; Xu, L.; Zhao, S. Adsorption and Heterogeneous Oxidation of As(III) on
46 Ferrihydrite. *Water Res.* **2011**, *45*, 6496-6504.
47
48
49 25. Cao, C. Y.; Qu, J.; Yan, W. S.; Zhu, J. F.; Wu, Z. Y.; Song, W. G. Low-Cost Synthesis of
50 Flowerlike α -Fe₂O₃ Nanostructures for Heavy Metal Ion Removal: Adsorption Property and
51 Mechanism. *Langmuir* **2012**, *28*, 4573-4579.
52
53
54 26. Jin, Y.; Liu, F.; Tong, M.; Hou, Y. Removal of Arsenate by Cetyltrimethylammonium
55
56
57
58
59
60

- 1
2
3 Bromide Modified Magnetic Nanoparticles. *J. Hazard. Mater.* **2012**, 227-228, 461-468.
- 4
5 27. Niu, H. Y.; Wang, J. M.; Shi, Y. L.; Cai, Y. Q.; Wei, F. S. Adsorption Behavior of Arsenic onto
6 Protonated Titanate Nanotubes Prepared via Hydrothermal Method. *Micropor. Mesopor.*
7 *Mater.* **2009**, 122, 28-35.
- 8
9 28. Wang, Y.; Liu, W.; Wang, T.; Ni, J. Arsenate Adsorption onto Fe-TNTs Prepared by a Novel
10 Water-Ethanol Hydrothermal Method: Mechanism and Synergistic Effect. *J. Colloid*
11 *Interface Sci.* **2015**, 440, 253-262.
- 12
13 29. Liu, W.; Ni, J.; Yin, X. Synergy of Photocatalysis and Adsorption for Simultaneous Removal
14 of Cr(VI) and Cr(III) with TiO₂ and Titanate Nanotubes. *Water Res.* **2014**, 53, 12-25.
- 15
16 30. Xiong, L.; Yang, Y.; Mai, J.; Sun, W.; Zhang, C.; Wei, D.; Chen, Q.; Ni, J. Adsorption
17 Behavior of Methylene Blue onto Titanate Nanotubes. *Chem. Eng. J.* **2010**, 156, 313-320.
- 18
19 31. Chen, Q.; Peng, L. M. Structure and Applications of Titanate and Related Nanostructures. *Int.*
20 *J. Nano. Technol.* **2007**, 4, 44-65.
- 21
22 32. Sun, X.; Li, Y. Synthesis and Characterization of Ion-Exchangeable Titanate Nanotubes.
23 *Chem. Eur. J.*, **2003**, 9, 2229-238.
- 24
25 33. Chen, Q.; Zhou, W.; Du, G. H.; Peng, L. M. Trititanate Nanotubes Made via a Single Alkali
26 Treatment. *Adv. Mater.* **2002**, 14, 1208-1211.
- 27
28 34. Xiong, L.; Chen, C.; Chen, Q.; Ni, J., Adsorption of Pb(II) and Cd(II) from Aqueous
29 Solutions Using Titanate Nanotubes Prepared via Hydrothermal Method. *J. Hazard. Mater.*
30 **2011**, 189, 741-748.
- 31
32 35. Wang, C. T.; Ro, S. H. Nanoparticle Iron-Titanium Oxide Aerogels. *Mater. Chem. Phys.* **2007**,
33 101, 41-48.
- 34
35 36. Wang, T.; Liu, W.; Xiong, L.; Xu, N.; Ni, J. Influence of pH, Ionic Strength and Humic Acid
36 on Competitive Adsorption of Pb(II), Cd(II) and Cr(III) onto Titanate Nanotubes. *Chem. Eng.*
37 *J.* **2013**, 215-216, 366-374.
- 38
39 37. Brunauer, S.; Deming, L. S.; Deming, W. E.; Teller, E. On a Theory of the van der Waals
40 Adsorption of Gases. *J. Am. Chem. Soc.* **1940**, 62, 1723-1732.
- 41
42 38. Yu, J.; Yu, J. C.; Leung, M. K. P.; Ho, W.; Cheng, B.; Zhao, X.; Zhao, J. Effects of Acidic and
43 Basic Hydrolysis Catalysts on the Photocatalytic Activity and Microstructures of Bimodal
44 Mesoporous Titania. *J. Catal.* **2003**, 217, 69-78.
- 45
46
47
48
49
50
51
52
53
54
55
56
57
58
59
60

- 1
2
3
4
5
6
7
8
9
10
11
12
13
14
15
16
17
18
19
20
21
22
23
24
25
26
27
28
29
30
31
32
33
34
35
36
37
38
39
40
41
42
43
44
45
46
47
48
49
50
51
52
53
54
55
56
57
58
59
60
39. Turki, A.; Kochkar, H.; Guillard, C.; Berhault, G.; Ghorbel, A. Effect of Na Content and Thermal Treatment of Titanate Nanotubes on the Photocatalytic Degradation of Formic Acid. *Appl. Catal. B: Environ.* **2013**, *138-139*, 401-415.
 40. Zhao, W.; Zhang, J.; Zhu, X.; Zhang, M.; Tang, J.; Tan, M.; Wang, Y. Enhanced Nitrogen Photofixation on Fe-Doped TiO₂ with Highly Exposed (101) Facets in the Presence of Ethanol as Scavenger. *Appl. Catal. B: Environ.* **2014**, *144*, 468-477.
 41. Yu, J.; Xiang, Q.; Zhou, M. Preparation, Characterization and Visible-Light-Driven Photocatalytic Activity of Fe-Doped Titania Nanorods and First-Principles Study for Electronic Structures. *Appl. Catal. B: Environ.* **2009**, *90*, 595-602.
 42. Zhang, F. S.; Itoh, H. Photocatalytic Oxidation and Removal of Arsenite from Water Using Slag-Iron Oxide-TiO₂ Adsorbent. *Chemosphere* **2006**, *65*, 125-131.
 43. Serpone, N.; Lawless, D.; Khairutdinov, R. Size Effects on the Photophysical Properties of Colloidal Anatase TiO₂ Particles: Size Quantization versus Direct Transitions in This Indirect Semiconductor? *J. Phys. Chem.* **1995**, *99*, 16646-16654.
 44. Ohsaki, Y.; Masaki, N.; Kitamura, T.; Wada, Y.; Okamoto, T.; Sekino, T.; Niihara, K.; Yanagida, S. Dye-Sensitized TiO₂ Nanotube Solar Cells: Fabrication and Electronic Characterization. *Phys. Chem. Chem. Phys.* **2005**, *7*, 4157-4163.
 45. Ou, H. H.; Liao, C. H.; Liou, Y. H.; Hong, J. H.; Lo, S. L. Photocatalytic Oxidation of Aqueous Ammonia over Microwave-Induced Titanate Nanotubes. *Environ. Sci. Technol.* **2008**, *42*, 4507-4512.
 46. Zhang, Y.; Yang, M.; Dou, X. M.; He, H.; Wang, D. S. Arsenate Adsorption on an Fe-Ce Bimetal Oxide Adsorbent: Role of Surface Properties. *Environ. Sci. Technol.* **2005**, *39*, 7246-7253.
 47. Dou, X.; Zhang, Y.; Zhao, B.; Wu, X.; Wu, Z.; Yang, M. Arsenate Adsorption on an Fe-Ce Bimetal Oxide Adsorbent: EXAFS Study and Surface Complexation Modeling. *Colloid. Surface. A* **2011**, *379*, 109-115.
 48. D'Arcy, M.; Weiss, D.; Bluck, M.; Vilar, R. Adsorption Kinetics, Capacity and Mechanism of Arsenate and Phosphate on a Bifunctional TiO₂-Fe₂O₃ Bi-Composite. *J. Colloid Interface Sci.* **2011**, *364*, 205-212.
 49. Biesinger, M. C.; Payne, B. P.; Grosvenor, A. P.; Lau, L. W. M.; Gerson, A. R.; Smart, R. S. C.

- 1
2
3 Resolving Surface Chemical States in XPS Analysis of First Row Transition Metals, Oxides
4 and Hydroxides: Cr, Mn, Fe, Co and Ni. *Appl. Surf. Sci.* **2011**, *257*, 2717-2730.
5
6
7 50. Zhao, X.; Xia, D.; Zheng, K. Fe₃O₄/Fe/Carbon Composite and Its Application as Anode
8 Material for Lithium-Ion Batteries. *ACS Appl. Mater. Interfaces* **2012**, *4*, 1350-1356.
9
10
11
12
13
14
15
16
17
18
19
20
21
22
23
24
25
26
27
28
29
30
31
32
33
34
35
36
37
38
39
40
41
42
43
44
45
46
47
48
49
50
51
52
53
54
55
56
57
58
59
60



83x35mm (300 x 300 DPI)